International Journal of Thermophysics, Vol. 28, No. 4, August 2007 (© 2007)
DOI: 10.1007/s10765-007-0179-x

Inverse Radiation Problem for Determination of Optical Constants of Fly-Ash Particles

L. M. Ruan,[1,2] H. Qi,[1] W. An,[1] and H. P. Tan[1]

Received April 24, 2006

In this paper, a technique for determining the optical constants of fly-ash particles from spectral transmittance measurements is presented. Combined with the precise Mie theory and the Kramers–Kronig (KK) relation, the complex refractive index was estimated by the spectral transmittance distribution of a cloud of fly-ash particles in potassium bromide (KBr) pellets. The unique and multi-value problems are thoroughly investigated. Particular attention is given to the error analysis of the inverse procedure including the influence of the experimental precision, the numerical simulation of the KK relation, scattering theory, and the single-scattering approximation. Good agreement was obtained between the inverse simulation results and the known optical properties of ash particles available in the literature. At the same time, an experimental analysis for two kinds of ash particles is also presented, and their spectral complex refractive indices in the range (1.0–25 μm) are determined by the inverse model used in the present work.

KEY WORDS: fly-ash particles; inverse radiation problem; optical properties; transmittance measurements.

NOMENCLATURE

$A(\nu)$	$A(\nu)=ix^{-3}S_0=Ar(\nu)+iAi(\nu)$, complex function, which is satisfied with KK relations
D	particle diameter (m)
$f_v(D)$	particle volume fraction distribution function (μm^{-1})
g	asymmetry factor

[1] School of Energy Science and Engineering, Harbin Institute of Technology, 92 West Dazhi Street, Harbin 150001, P.R. China.
[2] To whom correspondence should be addressed. E-mail: ruanlm@hit.edu.cn

hw	photon energy, $hw = 1.24/\lambda$ (eV)
I	radiative intensity ($W \cdot m^{-2} \cdot sr^{-1}$)
L	path length (m)
m	$m = n - ik$, complex refractive index
N	number density of particles (μm^{-3})
P_n	nth Legendre polynomials
$P(D)$	size distribution function (μm^{-1})
Q_e	extinction efficiency
S_0	scattering amplitude function for the forward direction
x	$x = \pi D/\lambda$, size parameter of particle
λ	wavelength (μm)
ν	frequency (Hz)
κ	extinction coefficient (m^{-1})
κ_a	absorption coefficient (m^{-1})
κ_s	scattering coefficient (m^{-1})
τ	transmittance of particle suspensions
Φ	scattering phase function
ω	single-scattering albedo
Ω	solid angle

Subscripts

l	low frequency
h	high frequency
ν	monofrequency

1. INTRODUCTION

There are various particles in a broad range of applications, such as astrophysics, geophysics, optics, electromagnetics, microphysics, biology, colloidal chemistry, acoustics, military science, etc. Thermal radiation from particulate-dispersion media often plays an important role in industrial applications involving fluidized beds, oil and gas-fired furnaces, radiative burners, solid propellant rockets, gas turbine combustors, and internal combustion engines [1]. Dombrovsky [2] reviewed the radiation heat transfer in a cloud of these particles and provides important insights into the complexities and subtleties about a dispersed system with particles. An analysis of thermal radiative heat transfer in these applications or systems requires accounting for the effects of particulates, such as char, soot, and fly-ash, which are present in the system as combustion products [3]. Especially, the fine fly-ash carried in the combustion gases of furnaces fired with pulverized coal has a dominant influence on radiative transfer. Also, numerical studies of radiative heat transfer in coal-fired systems have

indicated that fly-ash may play an important role both by contributing to the radiative emission and by impeding the transport of flame radiation to the walls through scattering [4]. For this reason, it is necessary to have a knowledge about the radiative properties of such particles.

However, the predicted effects of fly-ash on heat transfer are strongly dependent on ash absorption and scattering coefficients used in the calculations. And these coefficients and scattering phase functions can be calculated from complex refractive indices (or optical constants). Thus, the complex refractive indices of particles are the basic parameters for investigating the characteristics of radiative heat transfer in the systems of interest. Meanwhile, in order to determine ash or soot particle sizes and concentrations from *in situ* laser light scattering and extinction measurements, the refractive indices of the particles are usually determined at the known conditions. The most important limitation of optical ash or soot characterization techniques is the uncertainty in the refractive index of ash or soot [5]. The use of different, yet reasonable, values of the index can lead to sizes that differ by 30% and concentrations that differ by a factor of three [6]. Similarly, the accuracy of radiative heat transfer calculations is degraded due to uncertainties in the spectral variation of the refractive index as well as its absolute value [7].

Control of industrial processes involving various particulate materials and also an analysis of the internal structure of such materials require knowledge of the refractive indices of the materials as a function of the emitted wavelength. The production of soot and ceramic aerosols of specified sizes and shapes as well as the fine particle control in the electronics industry require reliable methods for determining the optical properties of the particulates [8]. Thus, from the viewpoint of the industrial applications above, especially those concerned about the accurate simulation of radiative heat transfer, investigation of the optical constants of particles is of particular importance. The optical constants of particles are prerequisites for all further research on radiative heat transfer in the media of interest.

However, the complex refractive index of particles cannot be measured directly; it can only be calculated with the help of some experimental data and a corresponding inverse model. Over the last two decades, many theoretical models for determining the refractive indices of fly-ash particles have been developed and improved. A large number of investigations are available which are devoted to techniques to retrieve the optical constants of particles. For example, Gupta et al. [9] investigated the optical properties of the fly-ash thoroughly, repeated *in situ* measurements with great precision, and made laboratory measurements on fly-ash from different coals. As they pointed out, the differences of the available absorption index of fly-ash are due to the unburned char present

in the furnace. Goodwin et al. [10] calculated the radiative properties of fly-ash polydispersions, allowing for realistic wavelength-dependent optical constants that are taken from the optical constants of homogeneous bulk samples with compositions similar to those of fly-ash particles. Meanwhile, various combinations of experimental techniques have been employed to deduce the complex refractive indices, such as reflectance measurements, angular light-scattering measurements, and spectral transmittance measurements. Compared to other methods, the transmission technique applies to a wider range of particle sizes, makes the sample closer to that of a particulate nature, and requires relatively simple experimental instruments. It shows promise in the refractive index determination for a wide range of particulate materials.

Some researchers have reported complex refractive indices of various types of carbon and ash particles deduced from transmittance measurements on dilute liquid suspensions of the particles or solid pellets. For example, Jernings et al. [11] presented a method that took advantage of a transmittance spectrum to determine directly the absorptive index of the complex refractive index. For a small size parameter and dilute particle suspensions, the scattering of particles was neglected. Lee and Tien [7] established a combination of the Mie scattering theory and the Drude–Lorentz dispersion model to deduce soot optical properties from *in situ* flame transmission data of a diffusion flame. Ku and Felske [12] presented a transmission method based on Rayleigh approximate scattering theory, and constructed a complex function, $A(\nu)$, that satisfied the dielectric dispersion Kramers–Kronig (KK) relation. But this approximation is only assumed to be accurate for a size parameter x up to 0.3. In subsequent work, Felske and Ku [13] proposed a technique to determine the spectral refractive indices, the size, and number density of soot particles from light scattering spectral extinction measurements in flames. Yu et al. [14] adopted a simplified Mie scattering theory to extend the applicable size parameter range to 0.7. Ruan et al. [15] presented a transmittance technique combined with Mie theory to investigate the radiative properties of particles and bulk material. Recently, Chen et al. [16] proposed a novel method for predicting the optical constants and the radiative properties of metals and heat mirror films by introducing an expression for the damping frequency in the Drude model. Dombrovsky et al. [17] studied experimentally the absorption spectra of several types of diesel fuel for which the refractive index is calculated using the substractive KK analysis. The radiative properties of diesel fuel droplets were calculated using the Mie theory and a simplified approach, based on approximations of absorption and scattering efficiency factors, which are sufficient for practical applications in the visible and infrared ranges. Ayranci et al. [18] developed an

inversion scheme based on tomographic reconstruction of flame emission spectra for *in situ* characterization of soot temperatures and volume fraction fields within an optically thin axisymmetric flame by extracting characteristic information on the soot refractive index from spectral gradients of emission spectra.

In this paper, a technique is presented such that the complex refractive indices of particles are deduced from the measured transmittance spectrum of a dilute monodispersion by use of the precise Mie theory and the Kramers–Kronig relation. The model has high precision, good adaptability, and a wide range of applications. The emphasis of this paper is the investigation of the unique and multi-value problems of the complex refractive index which is more important for the inverse model. The detailed theory and numerical simulation of the inverse model are described in Sections 2 and 3, respectively. Then, after describing in detail the effect of the primary errors on the accuracy of the refractive indices in Section 4, the experimental results and calculations for some ash particles have been reported in Section 5. The main conclusions and ideas for future research are summarized in Section 6.

2. THEORETICAL ANALYSIS

2.1. Transmittance for a Cloud of Particles

The governing equation for radiative transfer in a cloud of ash particles is as follows:

$$\frac{dI_\nu}{ds} = -(\kappa_{a\nu} + \kappa_{s\nu}) I_\nu + \kappa_{a\nu} I_{b\nu} + \frac{\kappa_{s\nu}}{4\pi} \int_{\Omega_i} I_\nu(\Omega_i) \Phi_\nu(\Omega, \Omega_i) d\Omega_i \tag{1}$$

For a room-temperature optically thin cloud, the monofrequency transmittance τ_ν of dilute particle suspensions of collimated incidence can be expressed as follows:

$$\tau_\nu = \exp(-\kappa_\nu L) \tag{2}$$

where L is the path length and $\kappa_\nu = \kappa_a + \kappa_s$ is the monofrequency extinction coefficient that can be expressed as

$$\kappa_\nu = N \int_{D_{min}}^{D_{max}} \frac{1}{4} \pi D^2 P(D) Q_{e,\nu}(m, x) dD = 1.5 \int_{D_{min}}^{D_{max}} Q_{e,\nu}(m, x) \frac{f_\nu(D)}{D} dD \tag{3}$$

where $m = n - ik$ is the complex refractive index of the particles, N is the number density of the spheres, $P(D)$ is the size distribution function,

$f_v(D)$ is the particle volume fraction distribution function, $x = \pi D/\lambda = \pi D\nu/c$ is the size parameter of a particle at a wavelength λ (frequency ν), and D is the particle diameter. According to Mie scattering theory, the monofrequency extinction efficiency can be expressed as

$$Q_{e,\nu}(m, x) = 4\mathrm{Re}\{S_0(m, x)\}x^{-2} \tag{4}$$

where the symbol Re denotes the real part of a complex number and S_0 is the scattering amplitude function for the forward direction. The extinction efficiency for a monodispersion of spherical particles has a relationship with the transmittance of a cloud of particles as

$$Q_{e,\nu} = -\frac{4}{\pi D^2 NL}\ln\tau_\nu \tag{5}$$

So when x and other geometrical parameters of the cloud are known, the complex refractive index of particles has a relationship with the transmittance of the cloud. However, m is a complex number with two variables, the refractive index n and the absorption index k, so an additional condition is needed.

2.2. Kramers–Kronig Relation

Let $A(\nu)$ be a complex function, which is satisfied with the Kramers–Kronig (KK) relation [17,19];

$$A(\nu) = ix^{-3}S_0 = Ar(\nu) + iAi(\nu) \tag{6}$$

It should be noted from Eq. (4) that

$$Ar(\nu) = \mathrm{Re}(A(\nu)) = -\mathrm{Im}(S_0)x^{-3} \tag{7a}$$

$$Ai(\nu) = \mathrm{Im}(A(\nu)) = \mathrm{Re}(S_0)x^{-3} = Q_{e,\nu}/4x = -\frac{1}{\pi D^2 xNL}\ln\tau_\nu \tag{7b}$$

The symbol Im denotes the imaginary part of a complex number. According to the KK relation,

$$Ar(\nu) = \frac{2}{\pi}P\int_0^\infty \frac{\eta Ai(\eta)}{\eta^2 - \nu^2}d\eta \tag{8}$$

where the symbol P denotes the Cauchy principal value of the integral.

2.3. Inverse Model

The complex function y is defined as

$$y(x, m, \nu) = Ar(\nu) + iAi(\nu) - ix^{-3}S_0 = 0 \tag{9}$$

We can obtain Ai from τ_ν by Eq. (7b), then Ar from the KK relationship in Eq. (8). Then we can calculate the complex refractive index m by solving this nonlinear complex function for definite x and ν. S_0 is a complex function; in solving this function, Refs. 12 and 14 took advantage of the Rayleigh approximation and the simplified Mie approximation, respectively. In this paper, the Mie scattering theory is used directly to solve S_0 without any approximation [20].

3. NUMERICAL SIMULATION

3.1. Solution of KK Relation

The experiment data can be measured only in a finite frequency range $[\nu_l, \nu_h]$, however, there is a Cauchy integral over all frequencies in the KK relation, so the finite data must be extrapolated into both high (ν_h, ∞) and low frequency $(0, \nu_l)$ regions. According to dispersion theory,

$$\lim_{\nu \to 0} Ai(\nu) = C_l \nu, \qquad \lim_{\nu \to \infty} Ai(\nu) = C_h / \nu^3 \tag{10}$$

where C_l and C_h are material constants. If the spectral range of the measured data is sufficiently wide, we can obtain approximate formulas as follows:

$$\begin{aligned} &0 < \nu < \nu_l, \quad Ai(\nu) = C_l \nu \\ &\nu_h < \nu < \infty, \quad Ai(\nu) = C_h / \nu^3 \end{aligned} \tag{11}$$

where $C_l = Ai(\nu_l)/\nu_l$ and $C_h = Ai(\nu_h)\nu_h^3$. Thus, the measured data over a finite range can be extrapolated to all frequencies.

The extrapolated formulas, which are based on data in a finite range, must introduce some errors. Thus, the subtractive KK (SKK) relations are adopted [17];

$$Ar(\nu) = Ar(0) + Ar_l + Ar_h + \frac{2\nu^2}{\pi} P \int_{\nu_l}^{\nu_h} \frac{Ai(\eta)}{\eta(\eta^2 - \nu^2)} d\eta \tag{12}$$

where

(a) Ar_l, Ar_h are integral results in the lower and higher extrapolated frequency ranges, respectively,

$$Ar_l(\nu) = \frac{\nu C_l}{\pi} \ln\left(\frac{\nu - \nu_l}{\nu + \nu_l}\right) \tag{13a}$$

$$Ar_h(\nu) = \frac{\nu^3 C_h}{\pi}\left\{\ln\left(\frac{\nu_h + \nu}{\nu_h - \nu}\right) + \frac{0.6667\nu^3}{\nu_h^3} - \frac{2\nu}{\nu_h}\right\} \tag{13b}$$

(b) the integral in the experimental range $[\nu_l, \nu_h]$ is

$$P\int_{\nu_l}^{\nu_h} \frac{Ai(\eta)}{\eta(\eta^2-\nu^2)}d\eta = \left(\int_{\nu+\Delta\nu}^{\nu_h} + \int_{\nu_l}^{\nu-\Delta\nu}\right)\frac{Ai(\eta)}{\eta(\eta^2-\nu^2)}d\eta + \int_{\nu-\Delta\nu}^{\nu+\Delta\nu}\frac{Ai(\eta)}{\eta(\eta^2-\nu^2)}d\eta \tag{14}$$

for $\eta = \nu$, and there is a singular point. The integral in $[\nu - \Delta\nu, \nu + \Delta\nu]$ is calculated by the Cauchy principal value of the integral ($\Delta\nu$ is one microinterval), according to the Hilbert transform,

$$P\int_{\nu-\Delta\nu}^{\nu+\Delta\nu} \frac{Ai(\eta)}{\eta(\eta^2-\nu^2)}d\eta = \frac{Ai(\nu+\Delta\nu)}{(\nu+\Delta\nu)(2\nu+\Delta\nu)} - \frac{Ai(\nu-\Delta\nu)}{(\nu-\Delta\nu)(2\nu-\Delta\nu)} \tag{15}$$

We take advantage of the composite Simpson method to calculate the integral in $[\nu_l, \nu - \Delta\nu]$ and $[\nu + \Delta\nu, \nu_h]$.

(c) Determination of $Ar(0)$

$Ar(0)$ is a material constant. According to the Lorentz–Drude multioscillator model, for dielectric materials such as ash or coal, $0 < Ar(0) < 1$. Based on the complex refractive index of ash given in Ref. 21, the precise $Ai(\nu)$ can be calculated by Eq. (7b) for different selected diameters of particles. Then, for $Ar(0) = 0$, $Ar(\nu)$ can be simulated by the SKK relation of Eq. (12). Meanwhile, a precise $Ar(\nu)$ can be obtained from Eq. (7a). The standard deviation and average absolute error between the SKK relation simulating $Ar(\nu)$ and precise results are shown in Table I. It indicates that a suitable $Ar(0)$ is about 0.133. The results indicated that a suitable value of $Ar(0)$, for which both the real and imaginary parts are rational (such that both are positive values), is in a very narrow range.

By the above three steps, $Ar(\nu)$ can be determined. When Ar and Ai are determined, we can solve complex Eq. (9) to determine the complex refractive index. In this paper, an improved intercept method for solving a complex function is adopted. This method has some advantages: no need for the derivative of the function, easy convergence, a wide selection of initial values for iteration, etc.

Table I. Error in $Ar(\nu)$ Simulation Using the SKK Relation with $Ar(0)=0$

D (μm)	0.1	0.5	1.0	2.0	3.0	5.0
Standard deviation	0.1333	0.1328	0.1351	0.1384	0.1384	0.1361
Average absolute error	−0.1330	−0.1324	−0.1349	−0.1382	−0.1392	−0.1360

3.2. Uniqueness of Solution

One of the key methods for solving an inverse problem is to determine the suitable uniqueness range. Because of the complexity of the function $Ar(\nu)$, multiple solutions of (n, k) may satisfy the same transmittance at each frequency by solving the complex equation. However, the complex refractive index of a particle is unique; thus, the uniqueness range of a solution must be considered first. For a given size parameter x, the complex equation y is controlled by Ai and Ar. If Ai and Ar are given, and only one m is determined, the solution is called unique; otherwise, the solution is multi-valued. For a given size parameter, the contour chart of Ai and Ar is shown in Fig. 1, whose coordinates are the real index n and the imaginary index k.

For small x, both Ai and Ar varied with n and k smoothly and, obviously, there is only one crossing point between the two contour curves of Ai and Ar. It indicates that a unique m can be calculated for a given Ai and Ar. However, for large x and small k, Ai and Ar varied with n sharply, and there are several contour curves of Ai or Ar with the same value, and several crossing points along the contour curves of Ai and Ar. It indicates that multiple values of m can be obtained for the same Ai and Ar. Meanwhile, the iterative initial value for solving the complex equation can influence the results. When the initial value is near the true solution, a suitable value can be approached, even in the multi-value region. In order to avoid multi-values, the solution is started from a low frequency, at which the size parameter is sufficiently small to satisfy the uniqueness condition. Then the solved value (n, k) is treated as the initial value at the neighboring higher frequency. If the initial n and k have already approached the true value, rational results can be obtained for the continuity of n and k. Thus, the uniqueness character of the first calculated point is important. For example, we assume the diameter of a particle is $2\,\mu$m and the lowest frequency is 2.30607×10^{13} Hz; the size parameter is 0.4833, and thus it can satisfy the unique solution.

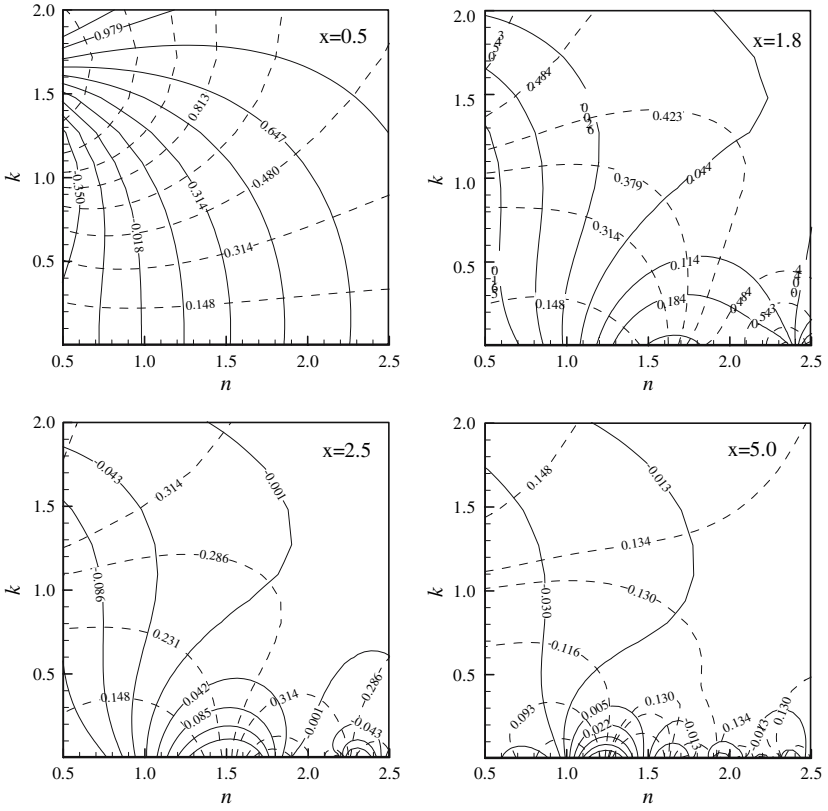

Fig. 1. Contour lines about *Ar* and *Ai*. *Ar*: —; *Ai*: - - - -.

4. ERROR ANALYSIS

The error analysis of a model is especially important to optimize the theory and experiment. Thus, the influence of several aspects on the present numerical model is thoroughly analyzed in this section. There are three steps in the simulation model: (a) calculating *Ai* by experimental transmittance, (b) calculating *Ar* using the KK relation, and (c) calculating S_0 using the Mie scattering theory and solving the complex equation *y*. There is almost no error in step c if both *Ai* and *Ar* are precise. The error in the theoretical model is mainly introduced by the errors in *Ai* and *Ar*. In the following sections, the complex index of ash [5] is adopted for the direct problem to calculate the extinction efficiency of particles with the Mie theory. Then they are treated as "experimental data" to substitute into our inverse model. Some errors were introduced artificially to analyze

the precision of our model. Because of the large value of the frequency ν, the photon energy ($hw = 1.24/\lambda$ eV, λ is the wavelength (μm)), which is proportional to the frequency, is employed instead of the frequency ν.

4.1. Influence of Ar

When both the complex index and size parameter are known, a precise Ai and Ar can be calculated with Eq. (5). By substituting them into our inverse model, a precise complex index can be obtained exactly, which indicates that the third step of our model is reliable. Thus, the error in our model is due to errors in Ai and Ar. We take a precise Ai and introduce an absolute error in Ar; the result is shown in Fig. 2. From this result, it can be seen that the error in Ar introduces an error in both n and k. When the absolute error for Ar is the same over the whole spectrum, the absolute error in n is almost the same over the whole frequency range. Positive errors in Ar introduce positive errors in n, negative ones introduce negative errors, and the two errors are approximately directly proportional. However, there is no obvious relation between the error in Ar and that in k.

4.2. Influence of Ai

This time, we take a precise Ar and introduce an absolute error in Ai; the inverse results are shown in Fig. 3. From these results, we can see that an error in Ai introduces only an error in k. When the absolute error in Ai is the same over the whole spectrum, the absolute error in k is almost the same over the whole frequency range. Positive errors in Ai result in positive errors in k, negative ones introduce negative errors, and the two errors are approximately directly proportional. However, almost no errors in n are introduced from errors in Ai. With an increase in the error in Ai when the relative error in k is about 1000%, the maximum relative error in n is only about 0.4%.

4.3. Influence of KK Relation

Because of the limitation of experiments, an extrapolation formula for the experimental data must be applied for calculation of the KK relation. For reducing this error, the subtractive KK relation is employed, but the error cannot be avoided. The influence of this error on the inverse model is analyzed in this paper. The extinction efficiency of a particle ($D = 1\,\mu$m) is calculated by means of the known complex refractive index of ash. Then we treat it by substituting the experimental data into our inverse simulation model. The results are shown in Fig. 4. For comparisons, the known

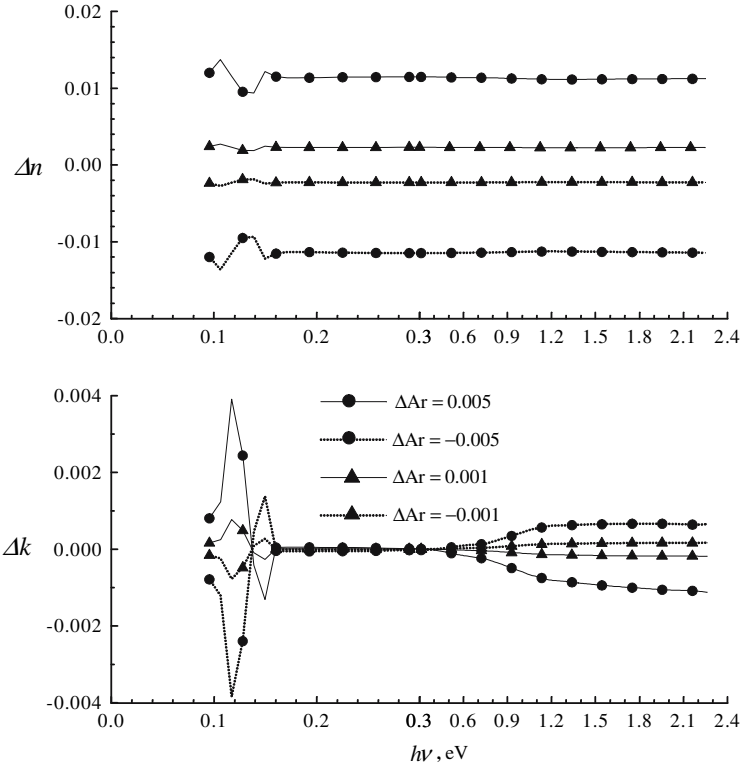

Fig. 2. Influence of *Ar* error on complex refractive index.

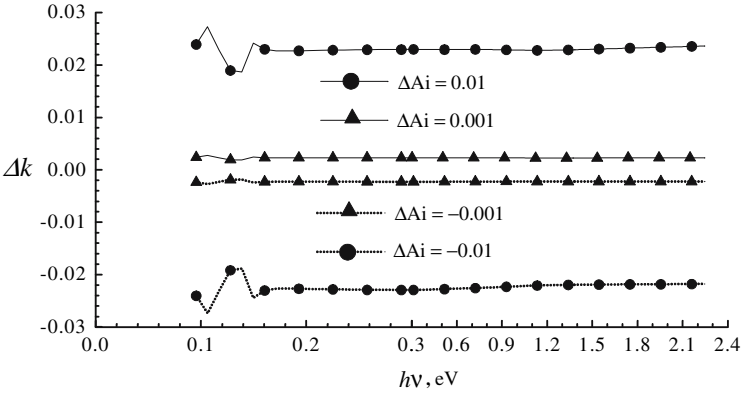

Fig. 3. Influence of *Ai* error on absorption index.

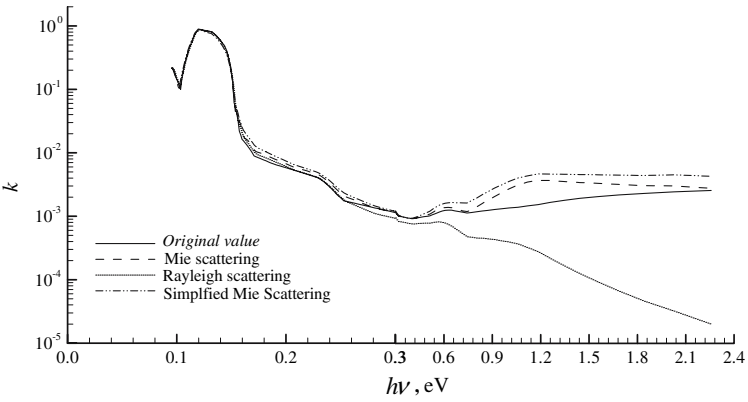

Fig. 4. Comparison between this model and the simplified method.

complex refractive indices and those calculated by the Rayleigh approximation model and simplified Mie scattering model are shown in this figure as well. It is worth noting that the precision of our model is higher than that of the other two models. Because the "experimental data" are precise (Ai is precise), the error can be only introduced from calculations using the KK relation (error in Ar).

4.4. Influence of Experimental Error

Except for the errors in the calculations discussed above, the error in the experiment is another factor that influences the precision of our model. In addition to the error in Ai introduced by neglecting multiscattering, the measurement error is another primary error source. During the experiment, several factors must be considered to minimize the errors, including the particle concentration of the cloud, the thickness of the presser bit, the diameter of the particles, the transmittance of the cloud, etc. Although there are some errors in each step, the last one is the major experimental error. Because Ar is calculated from Ai by the KK relation, an error in Ai must induce an error in Ar. So the experimental errors induce errors in both Ai and Ar. If other parameters are precise, the relative error of transmittance and the absolute error in Ai have the following relation: $\Delta Ai = \ln(1+\delta\tau) \approx \delta\tau$. In our calculations, first, we assume an absolute error in Ai, which is treated as an error of transmittance, then substitute Ai into the KK relation to calculate Ar, and finally, to calculate the complex refractive index. The results of our inverse simulation model are shown in Fig. 5.

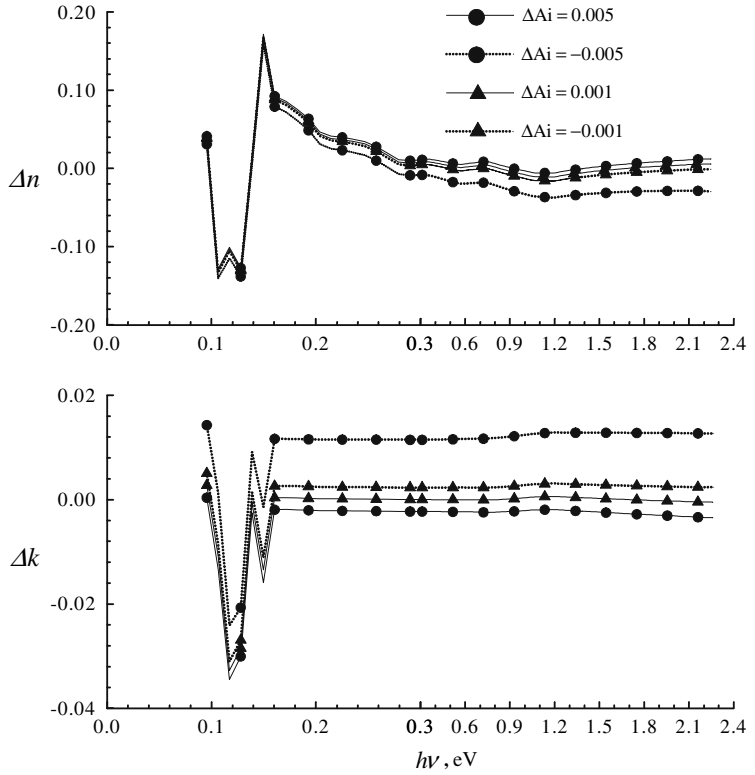

Fig. 5. Influence of transmissivity error on complex refractive index.

4.5. Influence of Multi-scattering

The inverse model is based on the assumption that multi-scattering is negligible. However, when the concentration of the cloud of particles and the scattering albedo ω are sufficiently large, this assumption will introduce some error. In fact, the relationship between the transmittance of the cloud and the extinction efficiency cannot be expressed simply as Eq. (1). The transmittance of the cloud has a relationship with not only the optical thickness, but also the scattering albedo and the scattering phase function of particles. So the assumption will introduce an error in calculating the extinction efficiency (error in Ai). The transmittance of a slab with multi-scattering particles is simulated by the Monte-Carlo model; the results are shown in Fig. 6, and those of a single-scattering model are also shown in this figure. In the high frequency range, both the size parameter and the scattering albedo of particles are large; thus, neglecting the multi-scattering

will introduce some transmittance error, which is also related to the concentration of the particles. With an increase in concentration, the error increases as well. In the low frequency range, two results are nearly identical for a small size parameter and scattering albedo, and it is reasonable to neglect the influence of multi-scattering in this range. In the meantime, a low concentration of particles in a cloud and a small cloud geometry size can also reduce the influence of multi-scattering. So, maintaining a dilute particle suspension is very important. To reduce the error introduced by a single-scattering approximation, a modified single-scattering method is employed, in which the equivalent extinction efficiency $Q_{e,d} = (1 - \omega g) Q_e$, instead of Q_e, is used where ω is the scattering albedo and g is the asymmetry factor. The parameters used in the calculations are as follows: the thickness of a slab is 0.6 mm, the diameter of the particles is 1 μm, and the range of the size parameter is [0.242, 5.712]; ω and g are shown in Fig. 7.

5. COMPLEX REFRACTIVE INDEX OF FLY-ASH

5.1. Experiment

In infrared spectrum analysis, the preparation and treatment of the test sample is extremely important. An unsuitable sample scheme cannot yield satisfactory results, even though the testing instrument is among the most reliable. The test sample in common use includes a pressed disk, liquid cell, or thin film. In our experiment, we employed the pressed disk method.

Because potassium bromide (KBr) is a nearly transparent medium in the infrared region, it is usually used as a spectrum medium in experiments. In our experiment, the pressed disk is made of a mixture of ash particles and KBr powder. Details of the experimental preparation and measurement procedure are given below:

(a) If the size of the KBr particles is not sufficiently small, the transparency of the pressed disk cannot be guaranteed. First, the powder of optically pure KBr must be lapped to produce a fine powder.
(b) Because a small size parameter can maintain the uniqueness of a solution (the smaller the diameter of an ash particle, the better), the diameter can reach 1–2 μm by means of lapping. A stereoscan photograph of the samples is shown in Fig 8.
(c) The mass ratio between the ash particles and KBr powder is determined by weighing; then, the number density of the ash spheres can be calculated if the density of ash, the density of KBr, and the diameter of the ash spheres are known. Then mix them sufficiently, taking

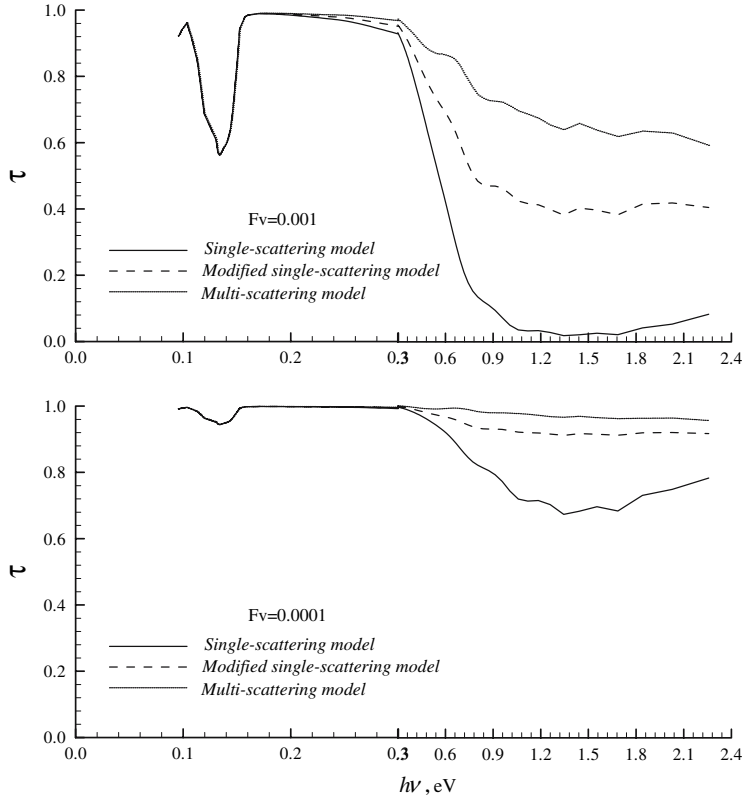

Fig. 6. Transmittance of one-dimensional slab.

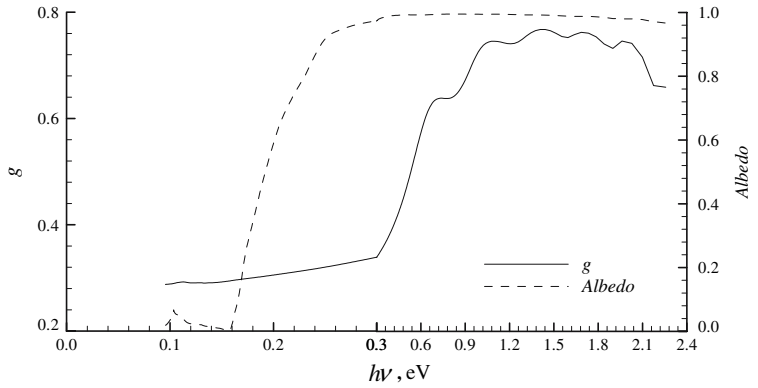

Fig. 7. Distribution of ω and g ($D = 1\,\mu$m).

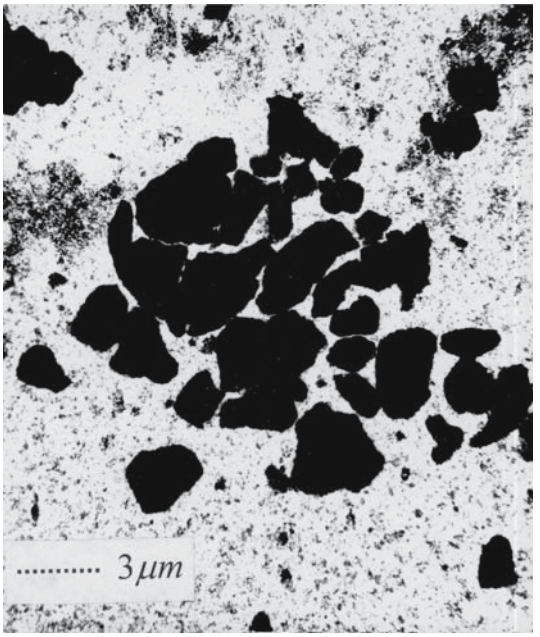

Fig. 8. Stereoscan photograph of the particles.

about 0.1 g mixture into the disk-forming machine and using a pressure of $200\,kg \cdot cm^{-2}$ to form a disk.

(d) Taking about 0.1 g of optically pure KBr powder into the disk-forming machine and using a pressure of $200\,kg \cdot cm^{-2}$, a reference disk whose thickness is the same as that of the sample disk is formed.

The transmittance of the disk was measured with a Fourier transform infrared optical spectrometer (Nicolet 60 SXB FT-IR), whose wavelength range is 1–25 μm. For reducing the influence of the KBr absorbance, first, the transmittance of the reference disk was measured, which is saved in the spectrometer, then the transmittance of the ash cloud can be determined directly, and the influence of KBr is reduced. In addition to the transmittance measurements, it is necessary to measure other non-radiative properties, such as the diameter of the particles, the density of the particles, and the thickness of the disk.

5.2. Simulation Results

The experiment and inverse simulation for coal ash and man-made ash, which have similar components to the actual ash, were carried out in

Table II. Components of Two Kinds of Ash

Components	SiO_2	Al_2O_3	Fe_2O_3	CaO	MgO	Na_2O	K_2O	TiO_2	SO_3
Ash	64.25	22.34	5.43	0.90	1.37	1.09	2.50	1.15	0.97
Man-made ash	68.14	23.69	5.76	0.95	1.46	0.00	0.00	0.00	0.00

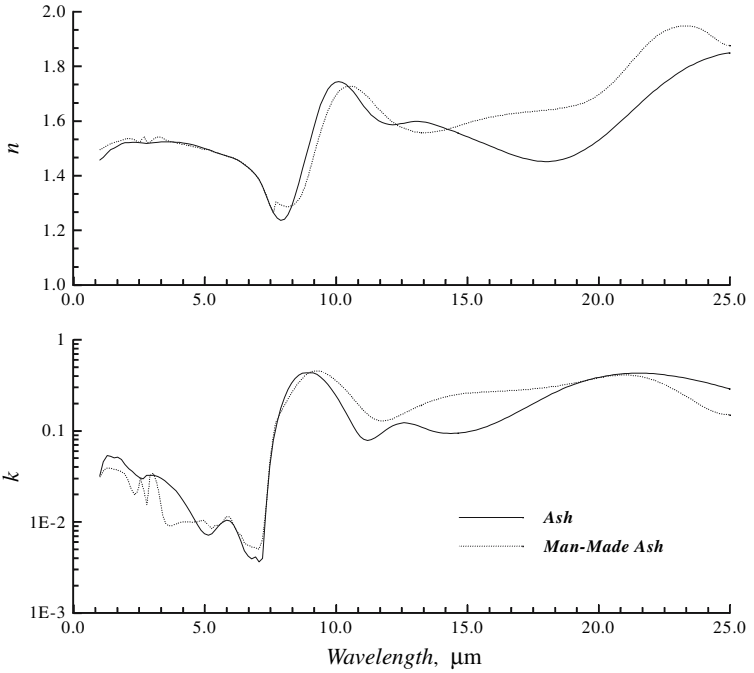

Fig. 9. Complex refractive index of ash and man-made ash.

this work. The components of both kinds of ash are shown in Table II. The simulation complex refractive indices are shown in Fig. 9.

From the experimental results and the simulation calculations of the fly-ash in the spectral range of (1.0–25 μm), the ash shows selective absorption in the infrared range: in the near infrared range of (1.0–8.0 μm), the absorption index k is quite small (about 10^{-2} order); however, in the range of (8.0–10.0 μm), an absorption peak exists with a peak of k (up to about 0.5). For ash particles, both the absorption index k and refractive index n vary with wavelength, as expected. Thus, the refractive index of ash could not be assumed to be a constant over the whole infrared range.

6. CONCLUSIONS

A technique has been presented for which the complex refractive indices of particles are deduced from the measured transmittance spectrum of a dilute monodispersion by use of the precise Mie theory and the Kramers–Kronig relation. Compared with other methods employed to determine the complex refractive indices, the present model has high precision, better adaptability, and a wide range of applications. By simulation of ash particles of known refractive indices and an experimental study of coal ash, the following conclusions are reached:

(a) Compared with the Rayleigh scattering model and the simplified Mie model, the present technique adopted the precise Mie theory and developed a new modified numerical method to solve the complex function, which resulted in the model having higher accuracy, a more unique solution, and wider applications.
(b) The computational errors of the present model have been thoroughly analyzed. When the scattering is strong and the particle concentration is large, certain errors may be introduced while neglecting multi-scattering. To reduce the error introduced by the single-scattering approximation, a modified single-scattering method is employed here. Meanwhile, since the spectral transmittance data may only be obtained over a finite range of wavelengths, the extrapolation of the KK theory will introduce some inherent error. However, high accuracy simulating methods (such as the solution of complex equations and the calculation of a forward amplitude function) can decrease the error of the numerical model.
(c) Considering the influence of experimental errors on the inverse model results, the errors in the spectral transmittance may influence the inverse results of k substantially but influence n only slightly.
(d) Finally, it should be emphasized that the technique developed here has higher accuracy, a more unique solution, and wider applications. Based on the present model, the refractive index inverse problem of high temperature particles may be investigated in future studies.

ACKNOWLEDGMENTS

The support of this work by the National Natural Science Foundation of China (No. 50576019) and the key project of the National Natural Science Foundation of China (No. 50336010) are gratefully acknowledged.

REFERENCES

1. R. Coquard and D. Baillis, *J. Thermophys. Heat Transfer* **19**:226 (2005).
2. L. A. Dombrovsky, *Radiation Heat Transfer in Disperse Systems* (Begell House, New York, 1996).
3. Y. L. Hua, G. Flamant, J. D. Lu, and D. Gauthier, *Int. J. Heat Mass Transfer* **48**:1145 (2005).
4. R. P. Gupta, T. F. Wall, and J. S. Truelove, *Int. J. Heat Mass Transfer* **26**:1649 (1983).
5. J. Widmann, J. C. Yang, T. J. Smith, S. L. Manzello, and G. W. Mulholland, *Combust. Flame* **134**:119 (2003).
6. J. D. Felske, P. F. Hsu, and J. C. Ku, *J. Quant. Spectrosc. Radiant Transf.* **35**:447 (1986).
7. S. C. Lee and C. L. Tien, in *Proc. Eighteenth Int. Symp. Combustion*, The Combustion Institute, Pittsburgh, Pennsylvania (1981), pp. 1159–1166.
8. B. K. Wiseman and J. A. Khan, in *Proc. 8th AIAA/ASME Joint Thermophys. Heat Transfer Conf.*, St. Louis, Missouri (2002), p. 3327.
9. R. P. Gupta and T. F. Wall, *Combust. Flame* **61**:145 (1985).
10. D. G. Goodwin and M. Mitchner, *Int. J. Heat Mass Transfer* **32**:627 (1989).
11. S. G. Jernings, R. G. Pinnick, and S. B. Gillespie, *Appl. Opt.* **18**:1368 (1979).
12. J. C. Ku and J. D. Felske, *J. Opt. Soc. Am. A* **3**:617 (1986).
13. J. D. Felske and J. C. Ku, *Combust. Flame* **91**:1 (1992).
14. Q. Z. Yu, H. P. Tan, and L. M. Ruan, *Int. J. Infrared. Millim. Waves* **12**:340 (1993).
15. L. M. Ruan, H. P. Tan, Q. Z. Yu, and M. Tang, in *Proc. Fourth Int. Symp. Adv. Sci. Technol. in the Far East*, Harbin, China (1995), pp. 247–250.
16. J. Chen and X. S. Ge, *Int. J. Thermophys*. **21**:269 (2000).
17. I Ayranci, R. Vaillon, N. Selcuk, F. Andre, and D. Escudie, in *Proc. Eurotherm 78-Computational Thermal Radiation in Participating Media II*, Poitiers, France (2006), pp. 307–316.
18. L. A. Dombrovsky, S. S. Sazhin, S. V. Mikhalovsky, R. Wood, and M. R. Heikal, *Fuel* **82**:15 (2003).
19. F. K. Kneubuhl, *Infrared Phys.* **29**:925 (1989).
20. C. F. Bohren and D. R. Huffman, *Absorption and Scattering of Light by Small Particles* (John Wiley & Sons, New York, 1983).
21. J. L. Ebert and S. A. Self, in *Proc. National Heat Transfer Conf.*, Paper HTD-106 (1989), pp. 123–126.